ORIGINAL PAPER

Fanglin Chen · Meilin Liu

Study of transition metal oxide doped LaGaO$_3$ as electrode materials for LSGM-based solid oxide fuel cells

Abstract Transition metal oxide doped lanthanum gallates, La$_{0.9}$Sr$_{0.1}$Ga$_{0.8}$M$_{0.2}$O$_3$ (where M = Co, Mn, Cr, Fe, or V), are studied as mixed ionic-electronic conductors (MIECs) for electrode applications. The electrochemical properties of these materials in air and in H$_2$ are characterized using impedance spectroscopy, open cell voltage measurement, and gas permeation measurement. Three single cells based on La$_{0.9}$Sr$_{0.1}$Ga$_{0.8}$Mg$_{0.2}$O$_3$ (LSGM) electrolyte (1.13 to 1.65 mm thick) but with different electrode materials are studied under identical conditions to characterize the effectiveness of the lanthanum gallate-based MIECs for electrode applications. At 800 °C, a single cell using La$_{0.9}$Sr$_{0.1}$Ga$_{0.8}$Co$_{0.2}$O$_3$ as the cathode and La$_{0.9}$Sr$_{0.1}$Ga$_{0.8}$Mn$_{0.2}$O$_3$ as the anode shows a maximum power density of 88 mW/cm^2, which is better than that of a cell using Pt as both electrodes (20 mW/cm^2) and that of a cell using La$_{0.6}$Sr$_{0.4}$CoO$_3$ (LSC) as the cathode and CeO$_2$-Ni as the anode (61 mW/cm^2) under identical conditions. The performance of LSGM-based fuel cells with MIEC electrodes may be further improved by reducing the electrolyte thickness and by optimizing the microstructures of the electrodes through processing.

Key words Lanthanum gallate · Mixed ionic-electronic conductor · Electrode materials · Solid oxide fuel cells

Abbreviations *LSC* La$_{0.6}$Sr$_{0.4}$CoO$_3$, La$_{1-x}$Sr$_x$CoO$_3$ · *LSGM* La$_{0.9}$Sr$_{0.1}$Ga$_{0.8}$Mg$_{0.2}$O$_3$ · *LSM* La$_{1-x}$Sr$_x$MnO$_3$ · *MIEC* Mixed ionic-electronic conductor · *SOFC* Solid oxide fuel cell · *TPB* Triple-phase boundary · *YSZ* Yttria-stabilized zirconia

F. Chen · M. Liu (✉)
School of Materials Science and Engineering,
Georgia Institute of Technology Atlanta,
GA 30332-0245, USA

Introduction

Because of their excellent oxide-ion conductivity and stability over a broad range of oxygen partial pressures, LaGaO$_3$-based electrolytes such as La$_{0.9}$Sr$_{0.1}$Ga$_{0.8}$Mg$_{0.2}$O$_3$ (LSGM) are considered to be a promising alternative to replace yttria-stabilized zirconia (YSZ) currently used in intermediate-temperature (600–800 °C) solid oxide fuel cells (SOFCs) [1–4]. The overall performance of an SOFC is determined by the electrochemical characteristics of each cell component, including the electrolyte, the cathode, the anode, and the interfaces between cell components. Accordingly, once a new electrolyte is identified, the development of appropriate cathode and anode materials compatible with the electrolyte becomes critical to the successful development of a new fuel cell system. Compared to high-temperature SOFCs based on YSZ electrolytes, the performance of intermediate-temperature SOFCs depends more on the electrode-electrolyte interfaces, since the interfacial polarization of a solid-state cell increases rapidly as the operating temperature is reduced [5].

The electrodes for SOFCs should have high electrical conductivity, high catalytic activities, adequate porosity for gas transport, and sufficient stability in contact with other cell components (electrolyte, interconnect, and current collector) under processing and operating conditions. Oxidation of oxygen at a cathode may involve the following steps: chemisorbing oxygen, reducing the chemisorbed oxygen to oxygen ions, and delivering the oxygen ions from the reaction sites to the electrolyte. If the cathode is a pure electronic conductor, oxygen reduction must take place at the triple-phase boundaries (TPBs) between gaseous O$_2$, the cathode, and the electrolyte. Traditionally, relatively thick and porous electrode/electrolyte composite films are employed to increase the number of TPB reaction sites; however, this also inevitably creates an additional tortuous pathway through which both ionic and electronic defects must travel. If the electrode is made of a mixed ionic-elec-

8

tronic conductor (MIEC), however, the reaction sites will be extended beyond the TPBs to the MIEC/gas interface [6]. When the ionic and electronic conductivities of the MIEC electrode are sufficiently high, electrode reactions may occur over the entire MIEC/gas interface, significantly increasing the number of reaction sites compared to electrodes of pure electronic conductors. Further, MIECs may exhibit higher catalytic activity because of the ability of transporting both ionic and electronic defects.

The perovskites $La_{1-x}Sr_xMnO_3$ (LSM) and $La_{1-x}Sr_xCoO_3$ (LSC) have been studied as cathode materials for LSGM-based SOFCs [7, 8]. While LSM is compatible with LSGM both chemically (insignificant interdiffusion) and thermally (similar thermal expansion coefficient), LSC is not suitable for the application owing to its considerable chemical interactions with LSGM and large mismatch in thermal expansion between LSC and LSGM. Owing to its limited ionic conductivity, however, LSM does not have adequate ambipolar conductivity to extend the reaction sites far beyond the TPBs [9]. Thus, MIECs with high ambipolar conductivities are needed to enhance the performance of the cathode. Similar to YSZ-based SOFCs, Ni-LSGM composite has been studied as the anode for LSGM-based SOFCs [8]. However, the observed anodic overpotentials were high and better anode materials are needed as well.

In this work, transition metal oxides are doped into $LaGaO_3$ with the intention to introduce electronic conduction while maintaining the existing ionic conduction. The resulting MIECs may be used as electrode materials for LSGM-based SOFCs. The use of these MIECs as electrode materials for LSGM-based SOFCs offers at least two advantages over the electrode materials studied. First, they are compatible both chemically and physically with LSGM electrolytes, minimizing interfacial reactions due to interdiffusion or chemical reaction. Second, they should have thermal expansion coefficients similar to that of LSGM, minimizing thermally induced stresses at the interface during thermal cycling and, thus, improving adhesion of the electrode to the electrolyte.

Oxides of Co, Mn, Cr, Fe, and V have been chosen as dopants to modify the properties of $LaGaO_3$. The selection of dopants is based on the variability of the valence of the transition metal and the similarity in ionic radii between the transition metal and gallium ion. Solubility of transition metal ions in $LaGaO_3$ and electrical properties of the doped $LaGaO_3$ materials are investigated in air and in hydrogen. Further, single fuel cells using LSGM electrolyte and transition metal oxide doped $LaGaO_3$ as electrodes are characterized to evaluate their suitability for electrode application.

Experimental

Sample preparation

$La_2(CO_3)_3 \cdot xH_2O$, Ga_2O_3, $SrCO_3$, and MgO were used as precursors for the preparation of $La_{0.9}Sr_{0.1}Ga_{0.8}Mg_{0.2}O_3$, while $CoCO_3 \cdot xH_2O$, $MnCO_3$, FeC_2O_4, Cr_2O_3, and V_2O_5 were used as sources of transition metal ions to form transition metal doped $LaGaO_3$ with an intended formula of $La_{0.9}Sr_{0.1}Ga_{0.8}M_{0.2}O_3$, where M represents Co, Mn, Fe, Cr, or V. Powders with stoichiometric composition were ball-milled in ethanol for 24 h and calcined at 1300 °C in air for 6 h to form the perovskite phase. X-ray powder diffraction (Philips, PW 1800) was used to monitor the phase composition of the calcined product. In cases of incomplete calcination, ball-milling and calcination were repeated until a pure perovskite phase was obtained. Powders with the perovskite phase were crushed using an agate mortar and pestle and then ball-milled in ethanol for 24 h. The resulting fine powders were pressed in pellets (diameter 20 mm and thickness 2–3 mm) and sintered at 1450 °C for 10 h. The densities of the sintered pellets were measured using the water-displacement technique. The sintered samples were polished, thermally etched, and then characterized using a scanning electron microscope (Hitachi S-800 SEM) to reveal the microstructures of the sintered samples.

Determination of total conductivity in a uniform atmosphere

Both surfaces of each sintered pellet were polished and ultrasonically cleaned before a paste of an Ag or Pt electrode was screen-printed on them. Pellets with printed electrodes were then fired at appropriate temperatures to form porous Ag or Pt electrodes. A computerized impedance analysis system, consisting of a Frequency Response Analyzer (Solartron 1255) and an Electrochemical Interface (Solartron 1286), was used to measure the impedance of the cells in the frequency range from 10 MHz to 1 mHz at temperatures ranging from 500 to 800 °C in air or H_2.

Characterization of ionic and electronic conductivity using a concentration cell

The ionic and electronic transference numbers were determined using the combination of impedance spectroscopy, open cell voltage measurement, and oxygen gas permeation measurement. Shown in Fig. 1 is a schematic arrangement for these measurements. Cells with Ag electrodes were attached to an alumina tube using a glass seal [10]. The glasses were fired in situ and the heating and cooling rates were carefully controlled to avoid cracking of the glass seal. The furnace was heated at 7 °C/min to 820 °C, held at that temperature for 10 min to soften the glass, and then cooled at 3 °C/min to the desired temperature for testing. Impedance spectra, open cell voltages, and oxygen permeation rates were measured under identical conditions on an oxygen concentration cell of air, $Ag|La_{0.9}Sr_{0.1}Ga_{0.8}M_{0.2}O_3$ (M = Mg, Co, or Mn)$|Ag$, Ar

The oxygen concentration of the incoming and outgoing gas was monitored using a YSZ oxygen sensor.

Fuel cell testing

Three kinds of fuel cells (named as cell 1, cell 2, and cell 3) using the LSGM electrolyte were tested. In cell 1, Pt was used as both cathode and anode (fired at 1000 °C for 2 h). In cell 2, $La_{0.6}Sr_{0.4}CoO_3$ was used as the cathode material and CeO_2-Ni was used as the anode material. The anode was prepared through in situ reduction of CeO_2/NiO composite [8] in order to form porous CeO_2 with metallic Ni particles on the walls of the porous channels. In cell 3, $La_{0.9}Sr_{0.1}Ga_{0.8}Co_{0.2}O_3$ was used as the cathode material and

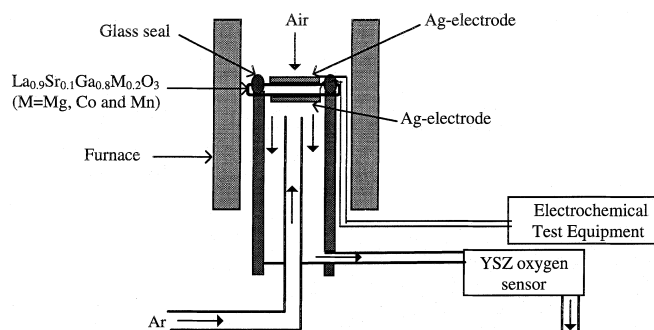Fig. 1 A schematic diagram showing the experimental arrangement for gas permeation, open-cell voltage, and impedance measurements

$La_{0.9}Sr_{0.1}Ga_{0.8}Mn_{0.2}O_3$ was used as the anode material. A slurry of each electrode material was obtained by mixing and grinding the powders with organic binder (Heraeus V-006) using a mortar and pestle. The electrode slurries were painted on the parallel surfaces of the LSGM pellet using a brush and then fired at 1100 °C for 2 h. A thin porous platinum layer was applied on the top of both electrodes to act as a current collector.

The configuration of the fuel cell is similar to that of the oxygen concentration cell shown in Fig. 1. After the glass seals were fired in situ, argon was supplied to the anode while the cathode was exposed to ambient air. Approximately 30 min after the cell reached the operating temperature, the anode gas was switched to hydrogen containing 2 vol% water vapor (hydrogen passing through water bubbler at ~20 °C) at a flow rate of 40 ml/min. Impedance spectra of the cells were measured after 30 min equilibrium at each operating temperature. Further, open cell voltages and current-voltage characteristics of the fuel cells were recorded (using EG&G Model 273 A) under identical conditions for each impedance measurement.

Results and discussion

Solubility of dopants

Compared to the X-ray diffraction (XRD) pattern of the $LaGaO_3$ perovskite phase shown in Fig. 2a, the XRD pattern of a sample with the intended composition $La_{0.9}Sr_{0.1}Ga_{0.8}Mg_{0.2}O_3$, shown in Fig. 2b, indicates that 10 mol% of La and 20 mol% of Ga ions may be substituted by Sr and Mg ions, respectively, without disturbing the perovskite structure. However, when 20 mol% of transition metal ions were introduced to substitute the Ga ions, shoulders at 58° and peak splitting at 68° were observed, as shown in Figs. 2c and 2d, indicating some distortion of the $LaGaO_3$ perovskite structure. Although it is still not clear, the probable cause of this lattice distortion includes (1) the difference in ionic radii between transition metal ions and Ga^{3+}, and (2) possible substitution of both Ga^{3+} and La^{3+} sites in the structure. Nevertheless, the essential features of the XRD patterns for transition metal oxide doped $LaGaO_3$ remain the same as those for $LaGaO_3$, indicating that single-phase perovskites with the formula $La_{0.9}Sr_{0.1}Ga_{0.8}M_{0.2}O_3$ (M = Co, Mn, Fe, Cr, and V) were obtained and 20 mol% of these transition metal oxides are soluble in $LaGaO_3$.
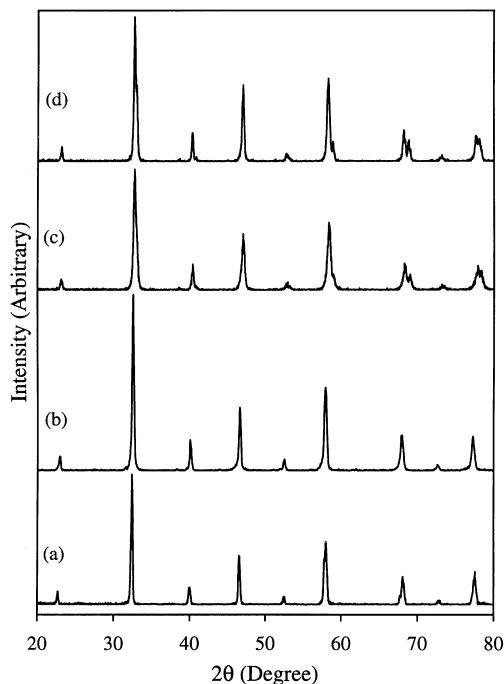

Fig. 2 X-ray diffraction patterns of a $LaGaO_3$, b $La_{0.9}Sr_{0.1}Ga_{0.8}Mg_{0.2}O_3$, c $La_{0.9}Sr_{0.1}Ga_{0.8}Co_{0.2}O_3$, and d $La_{0.9}Sr_{0.1}Ga_{0.8}Mn_{0.2}O_3$

Microstructure of sintered samples

Statistical analysis of the scanning electron microscopy (SEM) micrograph shown in Fig. 3a indicates that the porosity of the sintered $La_{0.9}Sr_{0.1}Ga_{0.8}Mg_{0.2}O_3$ sample is about 7.8%. Water-displacement measurements showed that the sintered $La_{0.9}Sr_{0.1}Ga_{0.8}Mg_{0.2}O_3$ sample has a density of about 92% of the theoretical one with negligible open porosity. Further, the open cell voltages of single fuel cells using $La_{0.9}Sr_{0.1}Ga_{0.8}Mg_{0.2}O_3$ as electrolytes were close to the theoretical values at 600–800 °C, implying that open porosity in the $La_{0.9}Sr_{0.1} Ga_{0.8}Mg_{0.2}O_3$ pellet is not significant. Thus, the pores observed on the SEM micrograph are mostly closed pores. The sintering densities of transition metal oxide doped samples, $La_{0.9}Sr_{0.1}Ga_{0.8}M_{0.2}O_3$ (M = Co, Mn, Cr, Fe or V), are greatly increased. Water-displacement measurements showed that these samples are more than 98% of the theoretical densities, indicating that transition metal ions act as a sintering aid to improve the sinterability of the materials. A typical SEM micrograph of a Mn-doped sample is shown in Fig. 3b.

Bulk conductivity in air

The impedance spectra of samples in the system $La_{0.9}Sr_{0.1}Ga_{0.8}M_{0.2}O_3$ (M = Mg, Co, Mn, Cr, or Fe) measured in air are more or less similar. They usually contain one or two semi-circles at the intermediate frequency range. Typical impedance spectra of a Co-doped sample ($La_{0.9}Sr_{0.1}Ga_{0.8}Co_{0.2}O_3$) measured at different

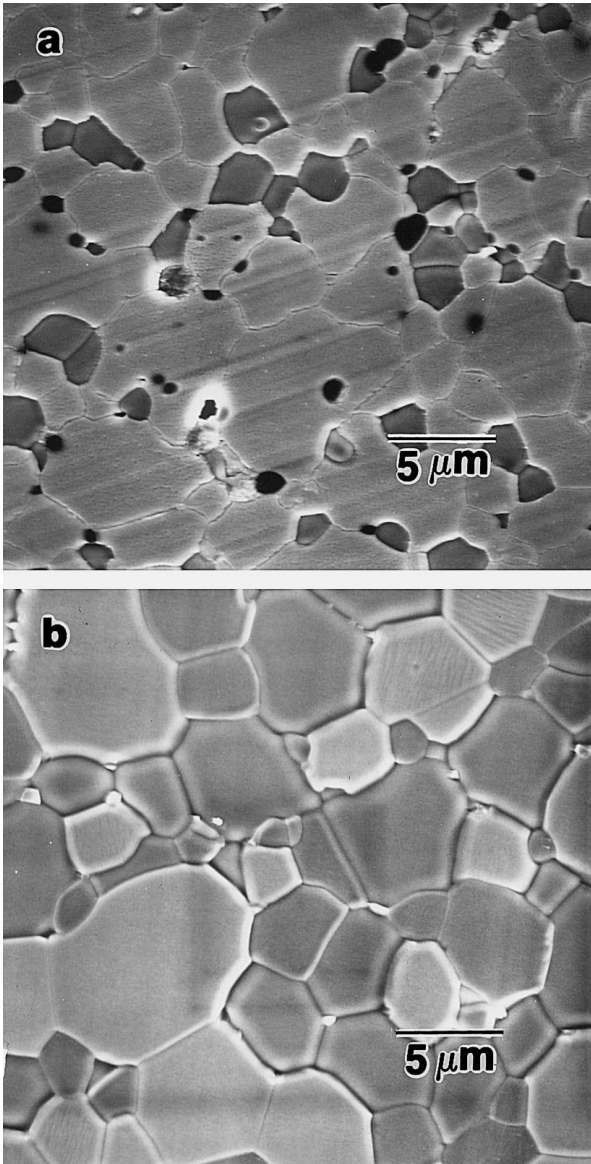**Fig. 3a,b** SEM micrographs of polished and thermally etched surfaces of two sintered samples: **a** $La_{0.9}Sr_{0.1}Ga_{0.8}Mg_{0.2}O_3$ and **b** $La_{0.9}Sr_{0.1}Ga_{0.8}Mn_{0.2}O_3$

Fig. 4a–c Typical impedance spectra of a $Pt|La_{0.9}Sr_{0.1}Ga_{0.8}M_{0.2}O_3|Pt$ cell measured at different temperatures: **a** $M = Co$, in air; **b** $M = Mn$, in H_2; and **c** $M = V$, in H_2
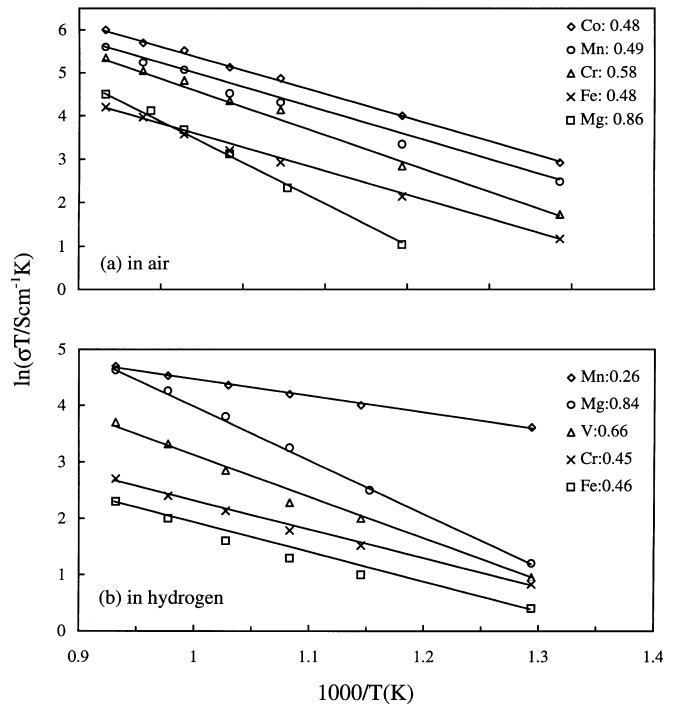
Fig. 5a,b Temperature dependence of the bulk conductivity of $La_{0.9}Sr_{0.1}Ga_{0.8}M_{0.2}O_3$: **a** $M = Mg$, Co, Mn, Cr or Fe, in air, and **b** $M = Mg$, Mn, V, Cr or Fe, in H_2. The value adjacent to each symbol is the activation energy in eV for electrical conduction in the material

temperatures in air are shown in Fig. 4a. The bulk resistance of the sample can be obtained from the intercept of the spectra with the real-axis at high frequencies. The temperature dependence of the bulk conductivities of different samples in the $La_{0.9}Sr_{0.1}Ga_{0.8}M_{0.2}O_3$ system in air is shown in Fig. 5a. It can be seen that introducing transitional metal ions in the Ga site in the $La_{0.9}Sr_{0.1}$-$Ga_{0.8}M_{0.2}O_3$ system increased the bulk conductivity compared to LSGM, especially at low temperatures. It is also noted that the activation energies for the samples with transitional metal ions in the Ga site are much smaller than that for LSGM. Among the transitional metals studied, Co and Mn doped samples exhibit much higher bulk conductivities in air than other samples. Accordingly, these two materials may be used as the cathode materials for LSGM-based SOFCs.
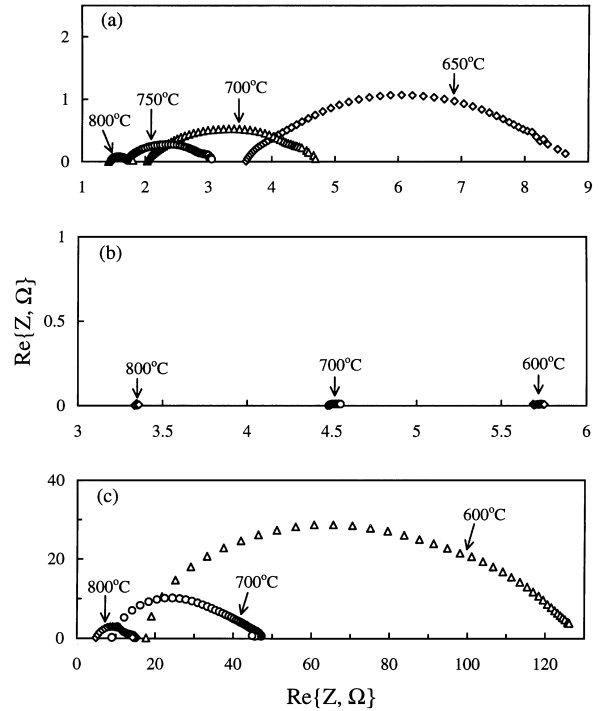
Bulk conductivity in H_2

Impedance spectra of transition metal oxide doped samples measured in H_2 are similar to those in air except for that of a Mn-doped sample ($La_{0.9}Sr_{0.1}Ga_{0.8}Mn_{0.2}O_3$). Typical impedance spectra of $La_{0.9}Sr_{0.1}Ga_{0.8}Mn_{0.2}O_3$ and $La_{0.9}Sr_{0.1}Ga_{0.8}V_{0.2}O_3$ measured in H_2 are shown in Figs. 4b and 4c, respectively. The spectra shown in Fig. 4b indicate that significant electronic conductivity exists in the Mn-doped sample. The bulk resistance of each sample in H_2 was determined from the intercept of the impedance spectra with the real-axis at high frequencies. The temperature dependence of the bulk conductivities of different samples in the $La_{0.9}Sr_{0.1}Ga_{0.8}M_{0.2}O_3$ system in H_2 is shown in Fig. 5b. It was observed that $La_{0.9}Sr_{0.1}Ga_{0.8}Mn_{0.2}O_3$ exhibits the highest bulk conductivity among the samples studied. Further, it is noted that $La_{0.9}Sr_{0.1}Ga_{0.8}Co_{0.2}O_3$ disintegrated under the testing conditions, indicating that $La_{0.9}Sr_{0.1}Ga_{0.8}Co_{0.2}O_3$ is not stable under a reducing atmosphere and thus cannot be used as anode material. The bulk conductivity of $La_{0.9}Sr_{0.1}Ga_{0.8}Mn_{0.2}O_3$ is 0.08 and 0.10 S/cm at 700 and 800 °C, respectively, and this material is chemically stable in an H_2 atmosphere. Therefore, it may be used as anode material for LSGM-based SOFCs.

Ionic and electronic conductivity

The ionic transference numbers, t_i, of $La_{0.9}Sr_{0.1}Ga_{0.8}M_{0.2}O_3$ (M = Mg, Co, or Mn) were determined from [11]

$$t_i = 1 - \frac{R_b}{R_t}\left(1 - \frac{V_{oc}}{E_N}\right) \tag{1}$$

where R_b and R_t are the bulk and total resistance, respectively, of the cell as determined from impedance spectroscopy, and V_{oc} and E_N are the open-cell voltage and Nernst potential across the cell, respectively.

Further, the ionic transference numbers, t_i, were also calculated from the combination of oxygen permeation and impedance measurements using the following equation (M. Liu, unpublished):

$$t_i = \left(1 - \frac{R_b}{R_t}\right) + \frac{R_b}{\left(\frac{E_N}{I_{O^{2-}}}\right)} \tag{2}$$

The ionic current due to the permeation of oxygen through the oxygen concentration cell, $I_{O^{2-}}$, can be calculated as [12]:

$$I_{O^{2-}} = \frac{85.89(V_2 X_2 - V_1 X_1)}{T} \tag{3}$$

where V_2 and V_1 are the flow rate (ml/min) of the outgoing and incoming gas, respectively, and X_2 and X_1 are the oxygen partial pressures (atm) of the outgoing and incoming gas, respectively.

Typical impedance spectra of cells using $La_{0.9}Sr_{0.1}Ga_{0.8}Co_{0.2}O_3$ and $La_{0.9}Sr_{0.1}Ga_{0.8}Mn_{0.2}O_3$ as the elec-
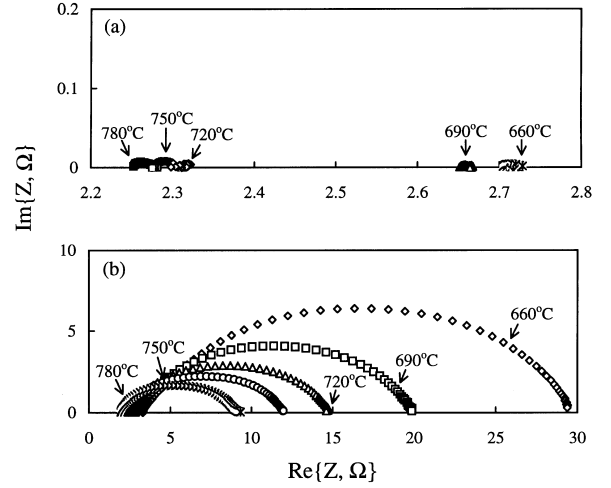

Fig. 6a,b Typical impedance spectra of an oxygen concentration cell with the configuration of Air, $Ag|La_{0.9}Sr_{0.1}Ga_{0.8}M_{0.2}O_3|Ag$, Ar measured at different temperatures: **a** M = Co and **b** M = Mn

trolyte measured at different temperatures are shown in Fig. 6. R_b and R_t are determined from the intercepts of the impedance spectra with the real-axis at high and low frequencies, respectively. The transference numbers of the three materials determined using Eqs. 1 and 2 are shown in Fig. 7. Figure 7a shows that $La_{0.9}Sr_{0.1}$-
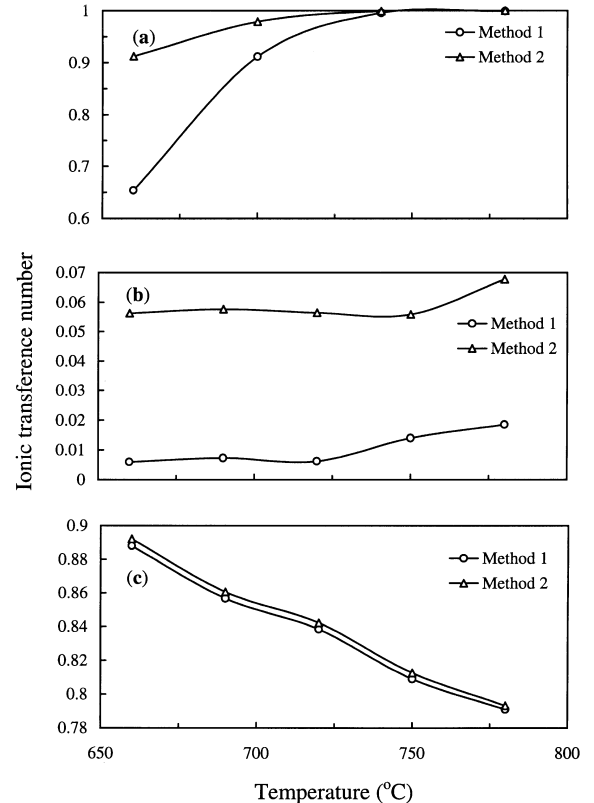

Fig. 7a,b Transference numbers of $La_{0.9}Sr_{0.1}Ga_{0.8}M_{0.2}O_3$ at different temperatures determined using method 1 (Eq. 1) and method 2 (Eq. 2): **a** M = Mg, **b** M = Co, and **c** M = Mn

$Ga_{0.8}Mg_{0.2}O_3$ exhibits predominantly ionic conduction at $T > 700$ °C, with the ionic transference number approaching 1 at 800 °C. As discussed elsewhere (M. Liu, unpublished) the uncertainty in both open cell voltage and gas permeation measurements increases with decreasing temperature, leading to larger discrepancies in the ionic transference number at low temperatures. For the cell using $La_{0.9}Sr_{0.1}Ga_{0.8}Co_{0.2}O_3$ as the electrolyte, the ionic transference number is less than 0.1, as shown in Fig. 7b, indicating that $La_{0.9}Sr_{0.1}Ga_{0.8}Co_{0.2}O_3$ exhibits predominantly electronic conduction. Since the open cell voltage in an oxygen concentration cell using $La_{0.9}Sr_{0.1}Ga_{0.8}Co_{0.2}O_3$ as the electrolyte is rather low (about 1 mV), the combination of gas permeation and impedance spectra is more reliable in determining the ionic transference number than the combination of open cell voltage and impedance spectra.

The electronic (R_e) and ionic (R_i) resistance of the electrolyte and the interfacial resistance R_p of the cell can be obtained from the following equations (M. Liu, unpublished):

$$R_e = \frac{E_N}{2I_{O^{2-}}} - \sqrt{\left(\frac{E_N}{2I_{O^{2-}}}\right)^2 - R_t\left(\frac{E_N}{2I_{O^{2-}}}\right)} \quad (4)$$

$$R_i = \frac{R_b R_e}{R_e - R_b} \quad (5)$$

$$R_p = \frac{E_N}{I_{O^{2-}}} - R_e - R_i \quad (6)$$

Table 1 summarizes R_e, R_i, and R_p for a cell using $La_{0.9}Sr_{0.1}Ga_{0.8}Mn_{0.2}O_3$ as the electrolyte. It is noted that R_p is much greater than both R_e and R_i. Therefore, the performance of the cell is dominated by the interfacial resistance. Accordingly, the observed open cell voltage was almost zero although the ionic transference number is as high as 0.8 at 780 °C, indicating that $La_{0.9}Sr_{0.1}$-$Ga_{0.8}Mn_{0.2}O_3$ is an MIEC with predominantly ionic conduction.

Similarly, Table 2 lists R_e, R_i, and R_p for the oxygen concentration cell using $La_{0.9}Sr_{0.1}Ga_{0.8}Co_{0.2}O_3$ as the electrolyte. It can be seen that R_e and R_p are much smaller than R_i, indicating that the interfacial resistance is not significant and electronic conduction predominates in this material.

Table 1 The electronic (R_e) and ionic (R_i) resistance of the electrolyte and the interfacial (R_p) resistance of the cell using $La_{0.9}Sr_{0.1}Ga_{0.8}Mn_{0.2}O_3$ as the electrolyte

Temperature (°C)	R_e (Ω)	R_i (Ω)	R_p (Ω-cm^2)
660	30.62	3.70	977.33
690	20.53	3.33	878.33
720	15.44	2.89	735.23
750	12.28	2.83	735.46
780	9.47	2.47	909.9

Table 2 The electronic (R_e) and ionic (R_i) resistance of the electrolyte and the interfacial (R_p) resistance of the cell using using $La_{0.9}Sr_{0.1}Ga_{0.8}Co_{0.2}O_3$ as the electrolyte

Temperature (°C)	R_e (Ω)	R_i (Ω)	R_p (Ω-cm^2)
660	2.81	47.08	8.01
690	2.87	46.90	9.77
720	2.88	48.18	8.51
750	2.38	40.26	19.27
780	2.43	33.56	18.08

Fuel cell performance

Shown in Fig. 8 are the current-voltage and current-power characteristics of the three single LSGM fuel cells using different electrode materials. It can be seen that the cell using MIEC electrodes exhibited much better performance than the one using Pt electrodes. The cell performance is also improved using MIEC electrodes compared to that of the cell using traditional electrodes (LSC as cathode and CeO_2-Ni as anode). At 800 °C, the
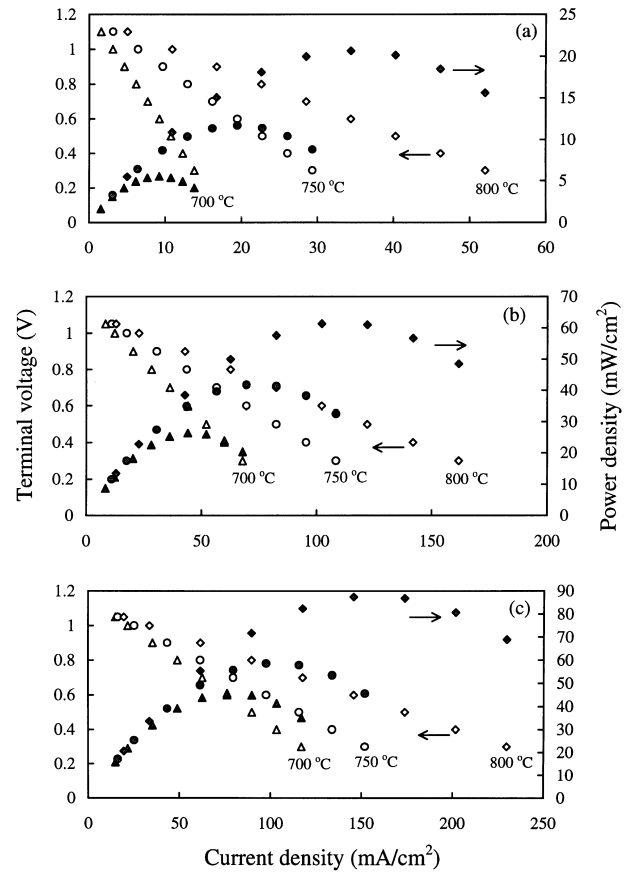

Fig. 8a–c Current-voltage and power-current characteristics of three single cells: **a** cell 1 (Pt|LSGM|Pt; electrolyte thickness: 1.13 mm, electrode area: 0.50 cm^2); **b** cell 2 (LSC|LSGM|CeO$_2$-Ni, electrolyte thickness: 1.58 mm, electrode area: 0.66 cm^2); and **c** cell 3 ($La_{0.9}Sr_{0.1}Ga_{0.8}Co_{0.2}O_3$|LSGM|$La_{0.9}Sr_{0.1}Ga_{0.8}Mn_{0.2}O_3$; electrolyte thickness: 1.65 mm, electrode area: 0.70 cm^2). *Open symbols* represent cell terminal voltages and *solid symbols* represent cell power densities
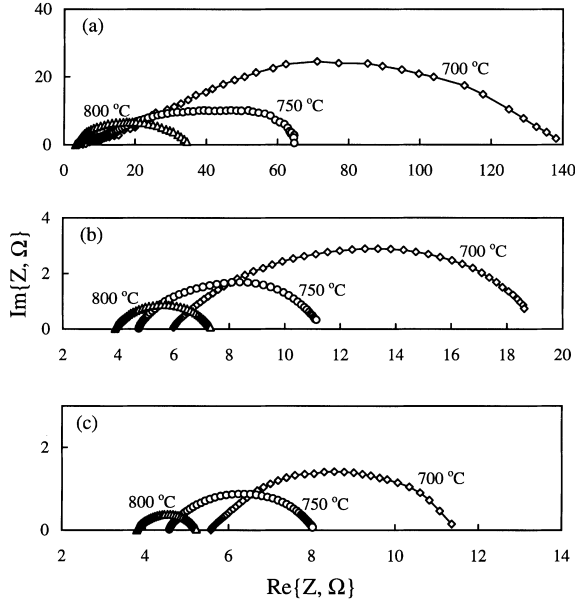
Fig. 9a–c Impedance spectra of **a** cell 1, **b** cell 2, and **c** cell 3 at different temperatures

Fig. 10a–c The bulk (R_b), total (R_t), and interfacial (R_p) resistance of **a** cell 1, **b** cell 2, and **c** cell 3 measured at different temperatures

maximum powder density of the cell with Pt electrodes was only 20 mW/cm^2 (corresponding to a current density of 34 mA/cm^2 at 0.6 V), and the maximum power density of the cell using LSC as the cathode and CeO$_2$-Ni as the anode was 61 mW/cm^2 (corresponding to a current density of 102 mA/cm^2 at 0.6 V), while the maximum power density of the cell with La$_{0.9}$Sr$_{0.1}$-Ga$_{0.8}$Co$_{0.2}$O$_3$ as the cathode and La$_{0.9}$Sr$_{0.1}$Ga$_{0.8}$Mn$_{0.2}$O$_3$ as the anode reached 88 mW/cm^2 (corresponding to a current density of 148 mA/cm^2 at 0.6 V). Accordingly, doped LaGaO$_3$ MIECs seems to be better electrode materials than Pt, LSC, or Ni composite for LSGM-based SOFCs.

Impedance spectra of the three cells at different temperatures are shown in Fig. 9. The interfacial resistance of the fuel cell (R_p) can be calculated from the following equation [11]:

$$R_p = \frac{R_t - R_b}{\frac{V_{oc}}{E_N}\left[\frac{1-R_b}{R_t}\left(1-\frac{V_{oc}}{E_N}\right)\right]} \qquad (7)$$

Figure 10 shows R_b, R_t, and R_p for the three cells at different operating temperatures. It can be seen that the R_p values of the cell with MIEC electrodes are smaller than the R_p values for the cell with Pt electrodes and for the cell with LSC as the cathode and CeO$_2$-Ni as the anode at all temperatures studied, indicating that using the MIECs as the electrode materials can reduce the interfacial resistance. It is also noted that, at $T \geq 750$ °C, R_p is smaller than R_b in the cell using MIEC as electrodes, implying that resistance of the electrolyte-electrode interfaces is not significant and the main power loss is due to the ohmic resistance of the electrolyte (with thickness of 1.65 mm).
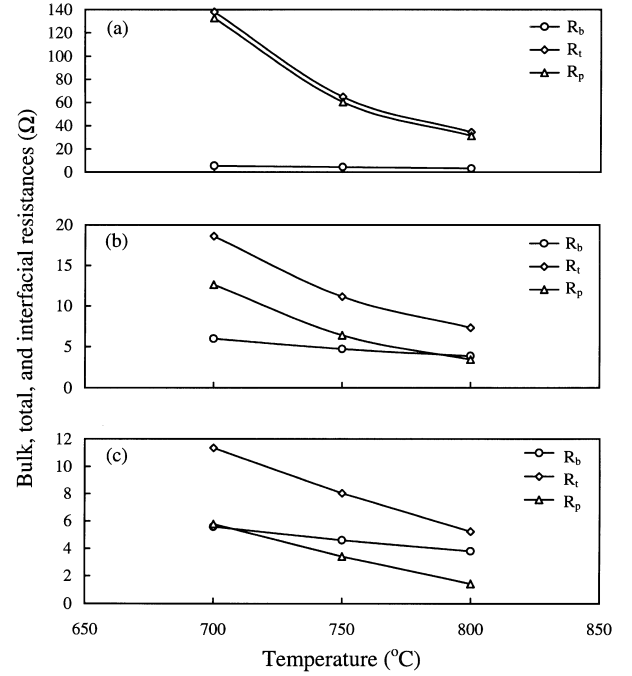
Using LSC as the cathode and CeO$_2$-Ni as the anode for a fuel cell with LSGM as the electrolyte (thickness 0.5 mm) operated at 800 °C, Huang et al. [8] obtained a maximum power density of 270 mW/cm2, whereas Ishihara et al. [13] reported a maximum power density of 710 mW/cm^2. From Figs. 8 and 10 it is noted that the LSGM-based cell using MIECs as electrodes has lower interfacial resistance and higher power densities than the cell using LSC as the cathode and CeO$_2$-Ni as the anode.

The electronic conduction in transition metal oxide doped LaGaO$_3$ originates from the multi-valence properties of the transitional metal ions. Accordingly, electronic conduction in these materials is a function of the dopant concentration of the transition metal ions, and it typically increases with dopant concentration within the solubility of the transition metal oxides in LaGaO$_3$. However, the solubility of transition metal oxides in LaGaO$_3$ and the optimum dopant concentration for electrode applications are yet to be determined. Consequently, it is expected that the performance of the LSGM-based fuel cells using MIECs as electrodes may be further improved by optimizing the dopant concentration and the microstructures of the MIEC electrodes through processing and by reducing the electrolyte thickness.

Conclusion

Transition metal oxide doped lanthanum gallates, La$_{0.9}$Sr$_{0.1}$Ga$_{0.8}$M$_{0.2}$O$_3$ (where M = Co, Mn, Cr, Fe or V), display not only higher conductivity but also better

14

sinterability than LSGM. Among the doped $LaGaO_3$ studied, Co-doped $LaGaO_3$ exhibits the highest conductivity in air and Mn-doped $LaGaO_3$ exhibits the highest conductivity in H_2, implying that the former may be used as a cathode whereas the latter may be used as a anode for LSGM-based SOFCs. Electrochemical measurements using an oxygen concentration cell indicate that $La_{0.9}Sr_{0.1}Ga_{0.8}Mn_{0.2}O_3$ is an MIEC with significant ionic conduction whereas $La_{0.9}Sr_{0.1}Ga_{0.8}Co_{0.2}O_3$ is an MIEC with overwhelming electronic conduction. At 800 °C, a single LSGM-based fuel cell using $La_{0.9}Sr_{0.1}Ga_{0.8}Co_{0.2}O_3$ as the cathode and $La_{0.9}Sr_{0.1}Ga_{0.8}Mn_{0.2}O_3$ as the anode shows a maximum power density of 88 mW/cm^2, which is better than those cells using Pt as both electrodes, or using LSC as the cathode and CeO_2-Ni as the anode under identical conditions. The performance of LSGM-based fuel cells with MIEC electrodes may be further improved by reducing the electrolyte thickness and optimizing the electrode processing.

References

1. Ishihara T, Matruda H, Takita Y (1994) J Am Chem Soc 116: 3801
2. Huang K, Feng M, Goodenough JB (1996) J Am Ceram Soc 79: 1100
3. Huang P, Petric A (1996) J Electrochem Soc 143: 1644
4. Stevensen JW, Armstrong TR, McCready DE, Pederson LR, Weber WJ (1997) J Electrochem Soc 144: 3613
5. Hu H, Liu M (1996) J Electrochem Soc 143: 859
6. Liu M (1998) J Electrochem Soc 145: 142
7. Huang K, Feng M, Goodenough JB, Schmerling M (1996) J Electrochem Soc 143: 3630
8. Huang K, Feng M, Goodenough JB, Milliken C (1997) J Electrochem Soc 144: 3620
9. Feng M, Goodenough JB, Huang K, Milliken C (1996) J Power Sources 63: 47
10. Agarwal V, Liu M (1997) J Electrochem Soc 144: 1035
11. Liu M, Hu H (1996) J Electrochem Soc 143: L109
12. Liu M, Joshi A (1991) In: Ramanarayanan TA, Tuller HL (eds) Proceedings of the 1st international symposium on ionic & mixed conducting ceramics. The Electrochemical Society, Pennington, N.J., p 231
13. Ishihara T, Minami H, Matsuda H, Nishiguchi H, Takita Y (1996) Denki Kagaku 64: 642